SUPPLEMENTAL MATERIAL

Loss of Protein Phosphatase 1 Regulatory Subunit PPP1R3A Promotes Atrial Fibrillation

Katherina M. Alsina PhD, Mohit Hulsurkar PhD, Sören Brandenburg MD, Daniel Kownatzki-Danger MS, Christof Lenz PhD, Henning Urlaub PhD, Issam Abu-Taha PhD, Markus Kamler MD, David Y. Chiang MD PhD, Satadru K. Lahiri PhD, Julia O. Reynolds BS, Ann P. Quick PhD, Larry Scott Jr. BS, Tarah A. Word PhD, Maria D. Gelves AS, Albert J.R. Heck PhD, Na Li PhD, Dobromir Dobrev MD, Stephan E. Lehnart MD, Xander H.T. Wehrens MD PhD

DETAILED METHODS

The data that support the findings of this study are available from the corresponding author upon reasonable request.

Statistical analysis. Unless otherwise specified in the figure legend, all supplemental data were analyzed using unpaired two-tailed Student's t-test for comparisons between two groups. The calcium data were analyzed using the Generalized Estimating Equation function in SPSS version 25.0.0.0, where mouse number was set as the subject variable, cell number as within subject variable, and each respective calcium measurement as the dependent variable. Genotype was the predictor factor. Statistics were performed using the Wald chi-square test with kernel quasi-likelihood. Alpha level was set at 0.05.

Generation of *Ppp1r3a*-KO mice. *Ppp1r3a*-KO mice were generated by CRISPR-Cas9 mediated deletion of exons 2 and 3 of the mouse *Ppp1r3a* gene. Guide RNA design and production were performed by the Mouse Embryonic Stem Cell Core at Baylor College of Medicine. Briefly, 5'-gRNA CTTTTCAGGTTTTAGTGATCTGG and 3'-gRNA GCTTGAGCCACAAGGCACTTTGG were selected using the Wellcome Trust Sanger Institute (WTSI) Genome Editing website (http://www.sanger.ac.uk/htgt/wge/).[1] C57BL/6J female mice, 24

to 32 days old, were injected with 5 IU/mouse of pregnant mare serum, followed 46.5 hr later with 5 IU/mouse of human chorionic gonadotropin. The females were then mated to C57BL/6J males, and fertilized oocytes were collected at 0.5 dpc. Next, sgRNA (10ng/ul) and Cas9 mRNA (100 ng/ul) in Rnase-free 1xPBS were microinjected into the cytoplasm of 100 pronuclear stage zygotes. Injected zygotes were transferred into pseudo-pregnant ICR females on the afternoon of the injection, approximately 25-32 zygotes per recipient female. Founder animals harboring the desired deletion were identified with primers P1 5'-CAAAAGCAAAGCAATCTCAGG, P2 5'-CATAAGTCTTCAGTGGTGACACAG and P3 5'-CCTCACTCTTCCAGCCCTCT. PCR reactions were done separately for the endogenous wild-type (WT) allele (using primers P1 and P2, expected DNA band size 493bp) and the interval deletion knockout (KO) allele (using primers P1 and P3, expected DNA band size ~297 bp). One founder animal was selected for breeding to establish the knockout line. Sanger sequencing confirmed the interval deletion. WT, heterozygous (HET), and KO mice were identified with the same primers used for founder screening. Schematic of the CRISPR-Cas9 approach and validation of the model can be found in **Supplemental Figure 1.**

Co-immunoprecipitation and mass spectrometry. Co-immunoprecipitation followed by mass spectrometry was carried out as previously described with few modifications[2]. Briefly, RyR2 was immunoprecipitated from lysate of WT mouse hearts using monoclonal antibody against RyR2 (MA3-916; Thermo Scientific, Waltham, MA). The same sample was immunoprecipitated with murine non-specific IgG (M5284; Sigma-Aldrich, St. Louis, MO) in parallel as negative control. Immunoprecipitates were separated on a short gradient SDS-PAGE gel and each lane was cut, trypsinized, and processed by tandem MS/MS mass spectrometry and analysis with the Maxquant software as described in detail previously.[3]

Co-Immunoprecipitation. Cardiac tissue samples were homogenized in 1% CHAPS in 500 μl RIPA buffer (pH 7.4) containing 150 mM NaCl, 10 mM Tis-HCl, 20 mM NaF, 1 mM $NaVO_3$ and protease and phosphatase inhibitor cocktails (cOmplete, Mini and PhosSTOP, Roche Applied Science, Penzberg, Germany). Preclearing was performed by adding 40 μl of Protein G Plus Agarose (Thermo Scientific) and samples were incubated on a rotator at 4ºC for 2 hours. Two μl of antibody: RyR2 antibody (MA3-916; Thermo Scientific), PP1c antibody (sc-6104; Santa Cruz Biotechnology, Dallas, TX), PPP1R3A antibody (sc-398425; Santa Cruz Biotechnology), mouse IgG (M5284; Sigma-Aldrich) or goat IgG (sc-2028; Santa Cruz Biotechnology) was added to the supernatant and the mixture was rotated overnight at 4 ºC. Then, 40 μl of protein G beads slurry was added and further incubated at 4 ºC for 1 hour. The pellet was collected and washed with 0.1% PBST twice. The pellet was then mixed with 20 μl loading buffer and incubated at room temperature for 30 minutes before being run on a SDS-PAGE gel.

Western blot analysis. Atrial and ventricular tissues were snap frozen in liquid nitrogen. Protein extraction and western blotting were performed as described.[4] In brief, atrial and ventricular lysates were subjected to electrophoresis on 5%, 10% or 15% acrylamide gels followed by transfer onto polyvinyl difluoride (PVDF) membranes. Primary antibodies against the following target proteins were then used to probe the membranes: PPP1R3A (1:1000; sc-398425; Santa Cruz Biotechnology for mouse samples), PPP1R3A (1:1000; NBP1-59934; Novus Biologicals, Centennial, CO for human samples), PPP1R3A blocking peptide MEPSEVPSQISKDNFLEVPNLSDSLCEDEEVTFQPGFSPQPSRRGSDSS (synthesized by Novus Biologicals), RyR2 (1:5,000; MA3-916; Thermo Scientific, Waltham, MA), RyR2 pS2814 (1:1,000; custom-made),[4] RyR2 pS2808 (1:1,000; custom-made),[4] PP1c (1:1,000; 1950-1; Epitomics, Burlingama, CA), PP2A (1:1,000; #610555; BD Biosciences, Franklin Lakes, NJ), SERCA2a (1:1,000; MA3-919; Thermo Scientific), CSQ (1:1,000; PA1-913; Thermo Scientific) PLN (1:1000; MA3-922; Thermo Scientific), PLN (1:1000; A010-14;Badrilla or ab92697;Abcam

for human), PLN pS16 (1:1000; A010-12AP; Badrilla, Leeds, United Kingdom), PLN pT17 (1:1,000; A010-13AP; Badrilla, Leeds, UK), PKA (1:1,000; 4782S; Cell Signaling Technologies, Danvers, MA), PKA pT197 (1:1000; 4781S; Cell Signaling) CaMKIIδ (1:1,000; S2169; Epitomics), CaMKIIδ pT286 (1:1000; 10011438; Cayman Chemicals, Ann Arbor, MI), LTCC (1:200; ACC-003; Alomone labs, Jerusalem, Israel) and GAPDH (1:10,000; MAB-374; Millipore, Burlington, MA). Membranes were then incubated with secondary anti-mouse antibody conjugated to Alexa-Fluor 680 (Invitrogen Molecular Probes) or with secondary anti-rabbit antibody conjugated to IR800Dye (Rockland Immunochemicals, Limerick, PA). Membranes were developed using a LICOR odyssey infrared imager. Signal intensities were quantified using Image J software.

Quantitative real-time PCR. Total RNA was isolated from heart tissues by TRIzol™ (#15596, Life Technologies, Carlsbad, CA) and Direct-zol™ (R2072, ZYMO Research, Irvine, CA), and was reverse transcribed by iScript™ (#1708841, Bio-Rad, Hercules, CA). Quantitative real-time (qRT)-PCR was conducted in triplicate in 96-well plates using PerfeCTa SYBR Green FastMix (Quanta Biosciences, Gaithersburg, MD) as described.[5] Relative mRNA transcript levels (normalized to RPL7) were calculated using the CT (cycle number) method and are reported as fold change. The primers used are listed in **Supplemental Table 7**.

EP Studies. *In vivo* electrophysiology (EP) studies were performed at 4-5 month old PPP1R3A KO and WT littermates as previously described.[6,7] Briefly, a 1.1 F octapolar catheter (EPR-800, Millar, Houston, TX) was inserted into the right atrium and ventricle via the external jugular vein of the anesthetized mouse. Simultaneous recording of surface ECG and intracardiac electrograms was acquired by IOX2.4 software (EMKA Technologies, Falls Church, VA). Baseline ECG parameters (RR, HR, PR, QRS, and QTc) were measured when mice reached 36.5°C. Body temperature was maintained between 36.5-37.0°C throughout the study by a heating device (Indus Instruments, Webster, TX) connected to the ECG board. Induction of atrial fibrillation was

assessed using an atrial burst pacing protocol as described in detail previously.[8] Briefly, a series of 2-second bursts were applied to the atrial tissue (stimulus duration = 1ms). The first 2-second burst had a cycle length (CL) of 40ms, and the CL of each successive burst was reduced by 2-ms decrements down to a CL of 20ms. AF inducibility was considered positive if at least 2 of 3 atrial burst pacing trials induced an AF episode lasting more than 1 second. The incidence of inducible AF was calculated as the number of mice with reproducible AF divided by the total number of mice studied in each group. Atrial weight (AW) and tibial length (TL) were evaluated at the conclusion of the study.

Transthoracic echocardiography. Functional echocardiographic studies were performed on *Ppp1r3a*-KO mice and their WT littermates between the ages of 4 and 5 months. Briefly, mice were anesthetized with 1.5% isoflurane in 100% O2 at 1.5 L/min. Vital signs were continuously monitored to ensure similar heart and respiration rates. Mice were kept on a heated platform to ensure body temperature was maintained between 36.5–37.5°C. Cardiac function was assessed using a VisualSonics VeVo 2100 Imaging System (VisualSonics, Toronto, Canada) equipped with a high-frequency MS505 probe. Images were acquired in M-mode at the mid-papillary level, as described in detail previously.[9]

Immunofluorescence STED nanoscopy. Cardiomyocytes were isolated from 14-week-old male wild-type mice on a C57BL/6N background based on a modified Langendorff perfusion protocol. Cardiac perfusion was performed initially using nominally Ca^{2+} free buffer (in mM: NaCl 120.4, KCl 14.7, KH2PO4 0.6, Na2HPO4 0.6, MgSO4 1.2, HEPES 10, NaHCO3 4.6, taurine 30, 2,3-butanedione-monoxime 10, glucose 5.5, pH 7.4 with NaOH) followed by collagenase type II containing buffer for digestion as previously described.[10,11]. Isolated ventricular and atrial myocytes were plated on coverslips coated with laminin and fixed in 4 % PFA for 5 min. Next, cells were incubated in blocking/permeabilization buffer overnight (10 % bovine calf serum, 0.2

% Triton in PBS). Primary antibodies were diluted in blocking buffer and incubated over night at 4 °C as follows: PPP1R3A 1:200 (sc-398425, Santa Cruz Biotechnology); RyR2 1:500 (HPA020028, Sigma-Aldrich); PLN 1:1000, kindly provided by Zhenhui Chen (Krannert Institute of Cardiology, Indiana University School of Medicine, USA). Subsequently, samples were washed three times in blocking buffer and incubated with secondary antibodies diluted 1:1000 for 2 h at room temperature: anti-mouse (STAR 635P, Abberior) and anti-rabbit (STAR 580, Abberior) for STED imaging; anti-mouse (Alexa Fluor 514, Thermo Fisher Scientific) and anti rabbit (Alexa Fluor 633, Thermo Fisher Scientific) for confocal imaging. For STED triple-immunofluorescence staining, RyR2 rabbit antibody was labeled with Zenon Alexa Fluor 488 rabbit IgG labeling kit as per the manufacturer's instructions (Thermo Fisher Scientific). After washing, samples were embedded in mounting medium (ProLong Gold antifade reagent, Thermo Fisher Scientific). For imaging we used a Leica TCS SP8 STED system with a HC PL APO C2S 100x/1.40 oil immersion objective: pixel size 16.23 x 16.23 nm, pixel dwell time of 400 ns, scanning speed 600 Hz, 32x line averaging; with white light laser excitation at 635 nm, 580 nm and 488 nm, and STED lasers at 775 and 592 nm. The power of STED laser beam was adjusted to optimize the STAR 635P, STAR 580, and Alexa Fluor 488 signal resolutions, respectively. Raw images were processed in ImageJ/Fiji (http://imagej.nih.gov/ij/), and image segmentation for binarized images included automatic local thresholding with the Bernsen algorithm after employing background subtraction and Gaussian blurring.

Histology. Whole hearts from *Ppp1r3a*-KO and WT mice were quickly excised, washed in normal saline, blotted dry and then fixed in 10% buffered formalin for 48 hours. After dehydration by immersion in an ethanol series, the samples were paraffinized using histoclear and paraffin washes. Longitudinal 7μm sections were cut, mounted onto slides, and deparaffinized. Sections were then stained with Masson trichrome (Thermo Fisher Scientific) and imaged on a light microscope to assess gross atrial morphology and atrial fibrosis. Fibrosis images were analyzed

using ImageJ software. The threshold tool was used to label the fibrotic tissue (blue staining), and the % of fibrosis was calculated by measuring the area fraction of labeled fibrotic tissue.

Confocal Ca^{2+} imaging. Confocal linescan imaging was performed on single atrial myocytes using a LSM880 confocal microscope (Carl Zeiss, Thornwood, NY) in line-scan mode. Briefly, murine atrial myocytes were isolated by retrograde Langendorf perfusion using a modified collagenase protocol as described.[4] Freshly isolated atrial myocytes were then incubated with 2 μmol/L Fluo-4-AM (Invitrogen, Carlsbad, CA) in normal Tyrode's solution containing 1.8 mmol/L Ca^{2+} for 30 minutes at room temperature. Fluo-4 loaded myocytes were placed in a chamber equipped with parallel platinum electrodes, and steady-state Ca^{2+} transients (CaT) were induced by 1-Hz pacing (5 ms, 10V). Pacing was then stopped for 20 seconds, during which time Ca^{2+} sparks were counted. Total SR Ca^{2+} content (SR load) was estimated by direct application of 10 mmol/L caffeine over the myocyte of interest. Activity of SERCA2a was calculated as the difference between the rate of decay of the pacing-induced CaT (which reflects Ca^{2+} extrusion by the combined activities of SERCA2a and NCX) and the rate of decay of the caffeine-induced CaT (which reflects Ca^{2+} extrusion by NCX only) as described.[12] Data were analyzed using Clampfit and Image J software with a SparkMaster plugin.

Complexome profiling and nanoLC-MS/MS analysis. A digitonin solubilized, enriched membrane faction of isolated cardiomyocytes from WT and PLN KO mice was separated on a 4-13% blue native PAGE gel as described.[13] Gel lanes were cut in 60 even pieces. After washing, gel slices were reduced with dithiothreitol (DTT), alkylated with 2-iodoacetamide and digested with Endopeptidase Trypsin (sequencing grade, Sigma-Aldrich) overnight. The resulting peptide mixtures were then extracted, dried in a SpeedVac, reconstituted in 2% acetonitrile/0.05%TFA acid/(v:v) and prepared for nanoLC-MS/MS as described.[14] Briefly, samples were enriched on a C18 precolumn (Dionex 5 x 0.3mm ID) and separated on an analytical reversed phase-C18

column (0.075 mm ID x 300mm, Reprosil-Pur 120 C18-AQ, 3 μL (Dr. Maisch, Baden-Wurttemberg, Germany) using a 46 min linear gradient of 5-40% buffer B (80% acetonitrile/0.08% formic acid (v:v) at 300 nl min^{-1}). The eluent was analyzed on a Q Exactive HF-X hybrid quadrupole/orbitrap mass spectrometer (ThermoFisher Scientific, Dreieich, Germany) equipped with a Flexlon nanoSpray source and operated under Xcalibur 4.1.31.9 software using a data-dependent acquisition method. Each experimental cycle was of the following form: one full MS scan across the 350-1600 *m/z* range was acquired at a resolution setting of 60,000 FWHM, and AGC target of 1*10e6 and a maximum 2*10e4 intensity threshold were then sequentially isolated at 1.4 FWHM isolation width, fragmented with nitrogen at a normalized collision energy setting of 30%, and the resulting product ion spectra recorded at a resolution setting of 15,000 FWHM, an AGC target of 2*10e5 and a maximum fill time of 54 ms. Selected precursor *m/z* values were then excluded for the following 20 s. Two technical replicates per sample were acquired. Technical replicates were normalized to each other using total area sums (TAS) from all slices per replicate from WT and PLN KO. Each protein migration profile was maximum normalized, over WT and PLN KO, and colored in the given look-up table using Microsoft Excel software. Mass spectrometric analysis of complexome data was performed by the core Facility Proteomics at the University Medical Center Gottingen and the Bioanalytical Mass Spectrometry group at the MPIbpc.

Data Processing. For complexome studies, raw data were processed using MaxQuant Software version 1.6.0.1. Proteins were identified against a UniProtKB-derived *Mus musculus* protein sequence database (v2016.04) along with a set of common lab contaminants. The search was performed with trypsin as enzyme and iodoacetamide as cysteine blocking agent. Up to two missed tryptic cleavages and methionine oxidation as a variable modification were allowed for. Instrument type ‘Orbitrap’ was selected to adjust for MS acquisition specifics.

Supplemental Table 1. Patient Characteristics for WB data

	SR	pAF	cAF
Patients, n	21	11	23
Gender, M/F	15/6	8/3	15/8
Age, y	70.4±2.4	71.8±2.1	70.1±1.8
Body mass index, kg/m^2 *	27.8±0.8	31.4±2.5	27.8±0.9
CAD, n (%)	8 (38)	4 (36)	4 (17)
AVD/MVD, n (%)	6 (29)	2 (18)	11 (48)
CAD+AVD/MVD, n (%)	7 (33)	5 (46)	8 (35)
Hypertension, n (%)	19 (90)	11 (100)	22 (96)
Diabetes, n (%)	9 (43)	3 (27)	10 (43)
Hyperlipidemia, n (%)	16 (76)	8 (73)	15 (65)
LVEF, %†	52.6±2.2	53.8±6.2	50.9±2.1
LA, mm‡	43.1±1.8	43.3±2.8	56.6±3.7*
Digitalis, n (%)	1 (5)	1 (9)	9 (39)*
ACE inhibitors, n (%)	11 (52)	8 (73)	12 (52)
AT1 blockers, n (%)	2 (10)	1 (9)	5 (22)
β-Blockers, n (%)	13 (62)	9 (81)	18 (78)
Dihydropyridines, n (%)	3 (14)	3 (27)	5 (22)
Diuretics, n (%)	5 (24)	7 (64)	12 (52)
Nitrates, n (%)	1 (5)	0 (0)	5 (22)
Lipid-lowering drugs, n (%)	13 (62)	7 (64)	8 (35)

Values are presented as mean±SEM or number of patients (%), SR, sinus rhythm as control; pAF, paroxysmal atrial fibrillation; cAF, chronic atrial fibrillation; CAD, coronary artery disease; AVD, aortic valve disease; MVD, mitral valve disease; LVEF, left

ventricular ejection fraction; LA, left atrial diameter; ACE, angiotensin converting enzyme; AT, angiotensin receptor; *P<0.05 *versus* SR from Chi-squared test for categorical variables. Either one-way Anova or Kruskal-Wallis test were used to analyze continuous variables. *Data were not available for 1 pAF and 1 cAF. †Data were not available for 2 SR, 6 pAF and 1 cAF. ‡Data were not available for 12 SR, 8 pAF and 13 cAF.

Supplemental Table 2. Patient Characteristics for Complexome Data

	SR	pAF	cAF
Patients, n	1	1	1
Gender, M/F	Male	Female	Female
Age, y	79	71	74
Body mass index, kg/m^2	24	29	24
CAD, n (%)	Yes	Yes	No
AVD/MVD, n (%)	No	No	Yes
CAD+AVD/MVD, n (%)	No	No	No
Hypertension, n (%)	No	Yes	Yes
Diabetes, n (%)	No	Yes	No
Hyperlipidemia, n (%)	No	Yes	Yes
LVEF, %	60	50	55
LA, mm	not available	not available	not available
Digitalis, n (%)	No	No	No
ACE inhibitors, n (%)	No	No	No
AT1 blockers, n (%)	No	No	No
β-Blockers, n (%)	No	Yes	Yes
Dihydropyridines, n (%)	No	No	No
Diuretics, n (%)	No	Yes	Yes
Nitrates, n (%)	No	Yes	No
Lipid-lowering drugs, n (%)	No	Yes	Yes

SR, sinus rhythm as control; pAF, paroxysmal atrial fibrillation; cAF, chronic atrial fibrillation; CAD, coronary artery disease; AVD, aortic valve disease; MVD, mitral valve

disease; LVEF, left ventricular ejection fraction; LA, left atrial diameter; ACE, angiotensin converting enzyme; AT, angiotensin receptor.

Supplemental Table 3. Primers for quantitative real-time PCR analysis of mouse heart tissue.

Name	Forward sequence (5' - 3')	Reverse sequence (5' - 3')
Ppp1r3a	GGAGCCAGAGCCTGTAAAGC	TGTTGGGATGTAGGACTCTGT
Col I	ACGGCTGCACGAGTCACAC	GGCAGGCGGGAGGTCTT
Col III	GTTCTAGAGGATGGCTGTACTAAACACA	TTGCCTTGCGTGTTTGATATTC
TGFB	CACCGGAGAGCCCTGGATA	TGTACAGCTGCCGCACACA
Cacna1C	TCCCGAGCACATCCCTACTC	ACTGACGGTAGAGATGGTTGC
Kcna5	CAATCAGGGGTCGCACTTCTC	ACAGTGGTCATAGTGACTACTGC
Kcnj3	GCCCAAGAAGAAACGGCAGC	CAGGGTAGTGAAGAGGTCCG
Kcnj5	CCGAGCGGGTCCACAACACC	TGCCTGCCTAAGCCTGGGGT

Supplemental Table 4. Phosphatases and kinases identified by mass spectrometry in RyR2 co-immunoprecipitation.

Protein names	Gene names	Anti-RyR2/ IgG†	LFQ Signal/ MW‡
Serine/threonine-protein phosphatase 1 catalytic subunit alpha/beta/gamma*	*Ppp1cb;Ppp1ca;Ppp1cc*	Infinity	15912
Serine/threonine-protein phosphatase 1 regulatory subunit 3A	*Ppp1r3a*	Infinity	8533
Serine/threonine-protein phosphatase 2 regulatory subunit A, alpha	*Ppp2r1a*	1.2	54554
cAMP-dependent serine/threonine-protein kinase catalytic subunit alpha/beta	*Prkaca; Prkacb*	10.1	10924
Serine/threonine-protein kinase mTOR	*Mtor*	9.3	1603
Striated muscle-specific serine/threonine-protein kinase	*Speg*	2.4	14080

*In this experiment, mass spectrometry was not able to distinguish between these three highly homologous PP1 catalytic subunits.

†Ratio of the mass spectrometry signal of each protein from the RyR2 immunoprecipitation versus that from the control IgG immunoprecipitation. The greater the ratio, the more likely the protein is a true interactor of RyR2. “Infinity” indicates that the protein is only identified and quantified in the RyR2 immunoprecipitation and not in the IgG immunoprecipitation.

‡Label-free quantification (LFQ) signal normalized to the molecular weight (MW) of each protein, as an estimate of the abundance of each protein in the RyR2 immunoprecipitation.

Supplemental Table 5. ECG parameters in anesthetized WT and *Ppp1r3a*-KO mice at 4 months of age.

	WT	KO	P value
Number of mice	12	10	
HR (bpm)	568 ± 16	598 ± 18	0.23
RR (ms)	106.5 ± 3.1	101.1 ± 2.6	0.21
PR (ms)	35.7 ± 0.5	34.1 ± 1.0	0.19
QRS (ms)	13.7 ± 0.3	13.1 ± 1.2	0.59
QT (ms)	23.4 ± 0.5	23.9 ± 0.4	0.54
QTc (ms)	2.3 ± 0.06	2.4 ± 0.04	0.19
AVERP (ms)	51.8 ± 3.8	50.1 ± 2.8	0.73
SNRT (ms)	131.3 ± 5.5	117.4 ± 3.9	0.06

HR, heart rate; bpm, beats per minute; QTc, corrected QT interval; AVERP, atrioventricular node effective refractory period; SNRT, sinoatrial node recovery time. Data represent mean±SEM.

Supplemental Table 6. **Echocardiographic analysis of WT and *Ppp1r3a*-KO mice at 4 months of age.**

	WT (n=4)	KO (n=4)	P value
HR (bpm)	545 ± 33.13	549 ± 28.05	0.9338
EDD (mm)	2.12 ± 0.11	2.10 ± 0.05	0.8575
ESD (mm)	3.35 ± 0.07	3.33 ± 0.03	0.8420
EF (%)	67.45 ± 3.44	68.18 ± 1.63	0.8555
FS (%)	36.81 ± 2.77	37.16 ± 1.26	0.9101
LVAWd (mm)	0.84 ± 0.00	0.83 ± 0.01	0.2255
LVAWs (mm)	1.11 ± 0.01	1.15 ± 0.04	0.3233
LVPWd (mm)	0.79 ± 0.03	0.73 ± 0.02	0.2241
LVPWs (mm)	1.09 ± 0.03	1.13 ± 0.03	0.3423

HR, heart rate; bpm, beats per minute; EDD, end-diastolic diameter; ESD, end-systolic diameter; EF, ejection fraction; FS, left ventricular fractional shortening; LVAWd, left ventricular anterior wall in diastole; LVAWs, left ventricular anterior wall in systole; LVPWd, left ventricular posterior wall in diastole; LVPWs, left ventricular posterior wall in systole. Data represent mean±SEM.

Supplemental Table 7. Characteristics of Ca^{2+} sparks in atrial myocytes from WT and *Ppp1r3a*-KO mice.

	WT	KO	P value
Number of cells	25	32	
Number of sparks	285	555	
Amplitude (F/F0)	0.60 ± 0.01	0.58 ± 0.01	0.188
FWHM (μm)	1.0 ± 0.03	1.09 ± 0.03	0.035
FDHM (ms)	16.6 ± 0.39	16.2 ± 0.27	0.498
TtP (ms)	15.3 ± 0.64	14.9 ± 0.47	0.673
dv/dt	70.5 ± 1.11	67.2 ± 0.81	0.016
Tau (ms)	17.0 ± 1.09	16.3 ± 0.59	0.532

FWHM, full width at half maximum; FDHM, full duration at half maximum; TtP, time to peak.

Data represent mean±SEM.

Supplemental Figure 1

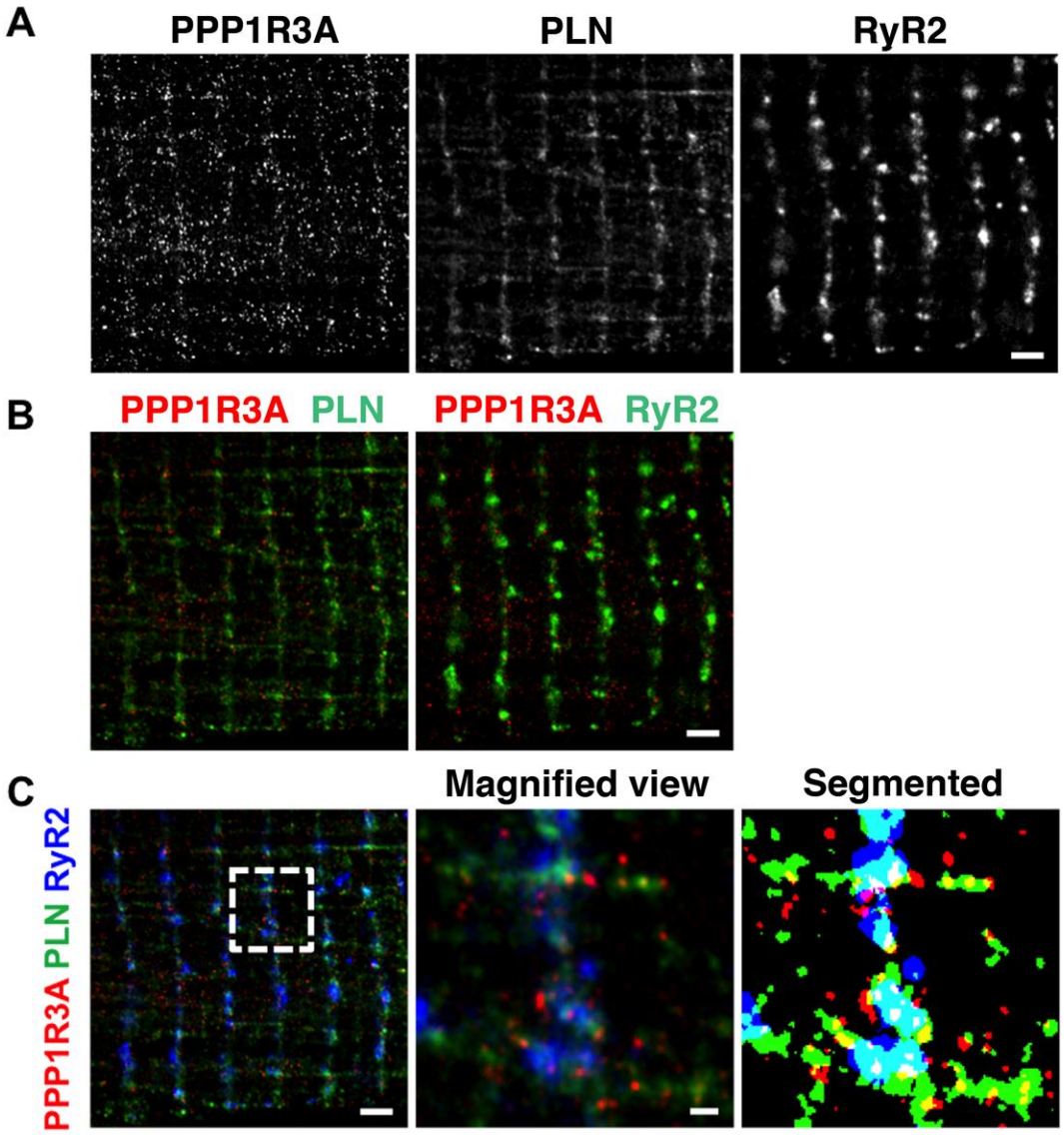

Triple-color STED imaging resolves discrete co-localization of PPP1R3A each with RyR2 and PLN. A, Single channel representation of a triple-immunostained mouse ventricular myocyte each for PPP1R3A, PLN and RyR2 (grey). Dual-color images in (**B**) show the relative signal distribution of PPP1R3A (red) relative to PLN (green) or RyR2 (green), respectively. **C**, Triple-color images identify PPP1R3A nanodomains (red) just adjacent to and overlapping each with the PLN (green) or RyR2 (blue) signals. To visualize the distinct local co-localization of PPP1R3A

either with PLN or RyR2, the magnified STED images were subjected to image segmentation. Dashed box indicates area of magnified view. Scale bars 1 µm (*left*) or 200 nm (magnified view).

Supplemental Figure 2

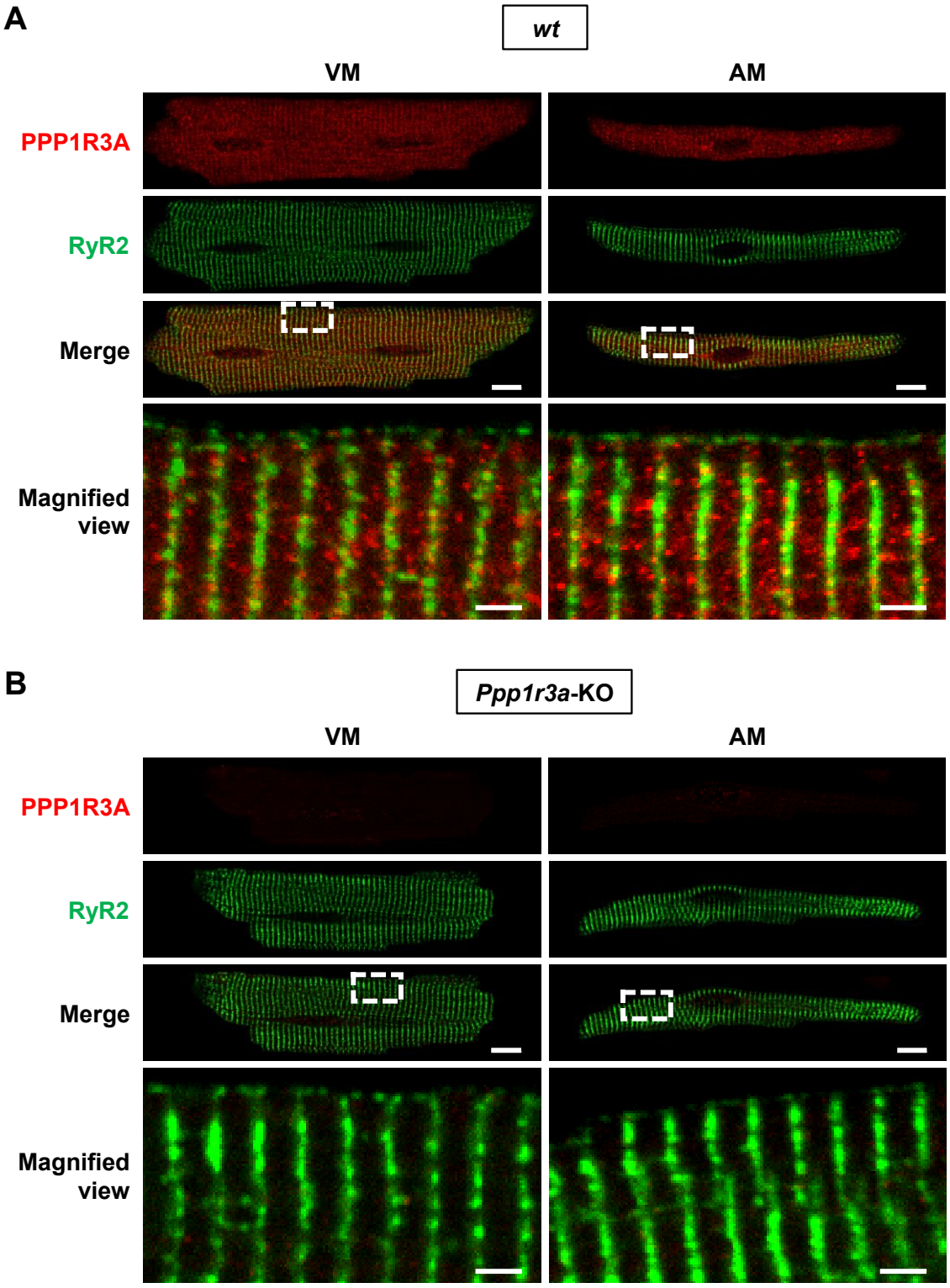

Validation of the signal specificity of the antibody against PPP1R3A in *Ppp1r3a-KO* cardiomyocytes. Isolated ventricular (VM) and atrial (AM) cardiomyocytes each from wild-type (**A**) and *Ppp1r3a*-KO hearts (**B**) were co-immunostained for PPP1R3A and RyR2 to confirm the PPP1R3A signal specificity. Dashed boxes indicate magnified views below. Scale bars indicate 10 µm in whole-cell images or 2 µm in image magnifications.

Supplemental Figure 3

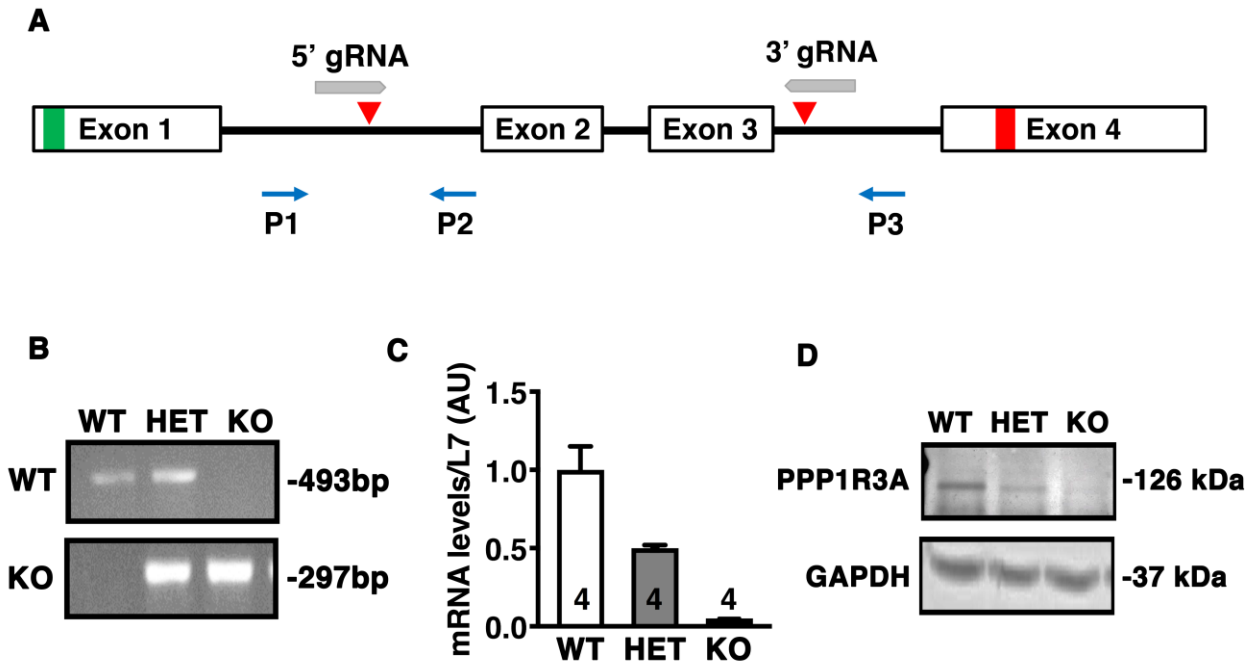

Generation and validation of *Ppp1r3a* KO mice. A, Schematic of mouse *Ppp1r3a* genomic DNA with gRNAs (in grey) blinding to regions flanking exons 2 and 3. Red triangles depict Cas9 cut sites. Blue arrows depict genotyping primers P1, P2 and P3. **B**, Genotyping results from *Ppp1r3a* WT, HET and KO mouse tails. Primers P1 and P2 amplify a 493bp fragment from WT mice, whereas P1 and P3 amplify a 297bp fragment from KO mice. **C**, Quantification of *Ppp1r3a* mRNA levels normalized to L7 in *Ppp1r3a* WT, HET and KO mouse hearts. **D**, Western blot images showing PPP1R3A protein expression in cardiac lysates from *Ppp1r3a* WT, HET and KO mice. AU, arbitrary units. Data represent mean±SEM.

Supplemental Figure 4

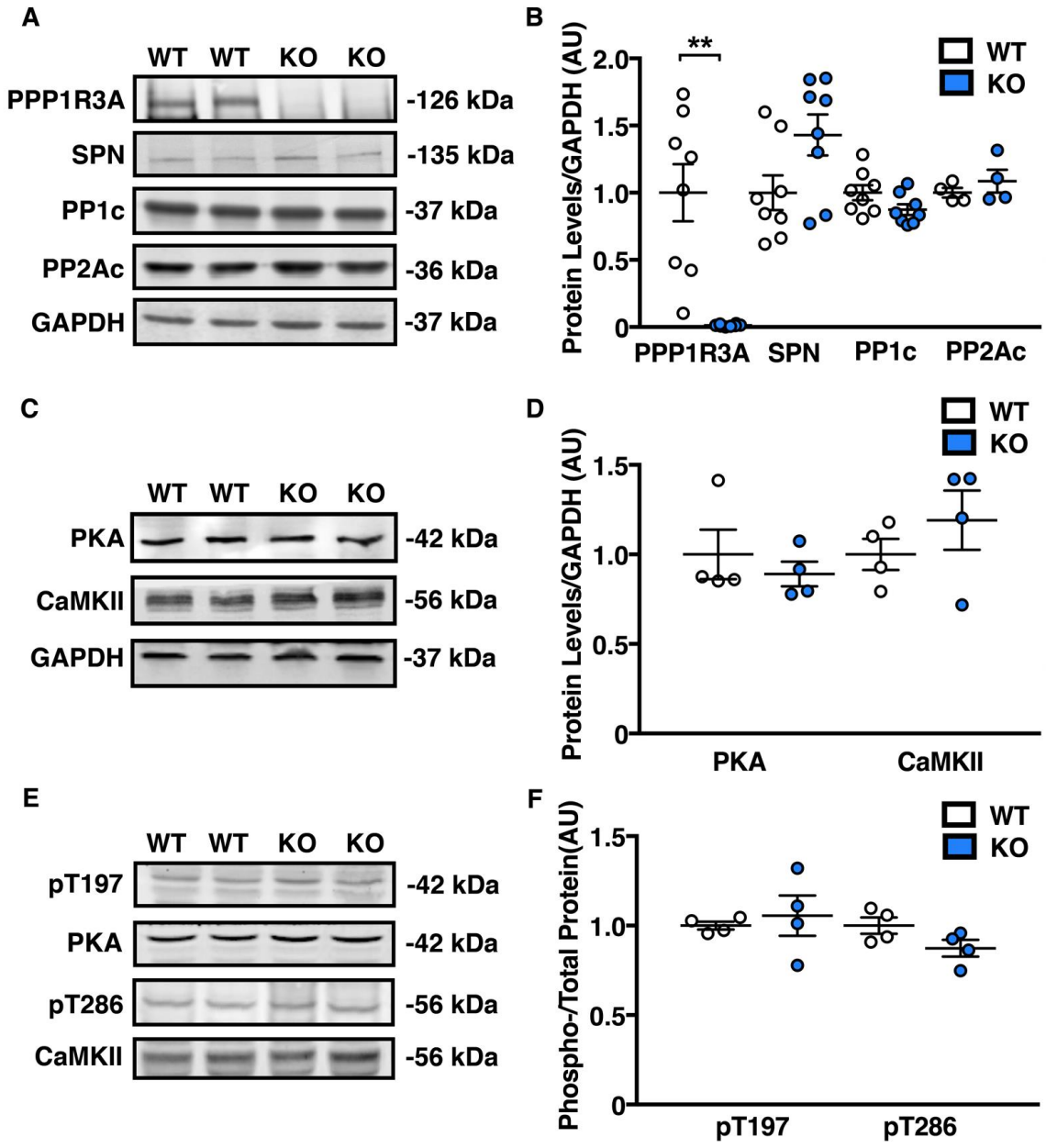

Unchanged levels of phosphatases and kinases in *Ppp1r3a* KO atria. Representative western blots and dot plots showing *Ppp1r3a* ablation has no effect on atrial expression levels of (**A** and **B**) spinophilin (SPN), PP1c, PP2Ac, (**C** and **D**) PKA and CaMKII, or (**E** and **F**) auto-phosphorylation sites of PKA and CaMKII. Data represent mean±SEM (**P<0.01 vs. WT).

Supplemental Figure 5

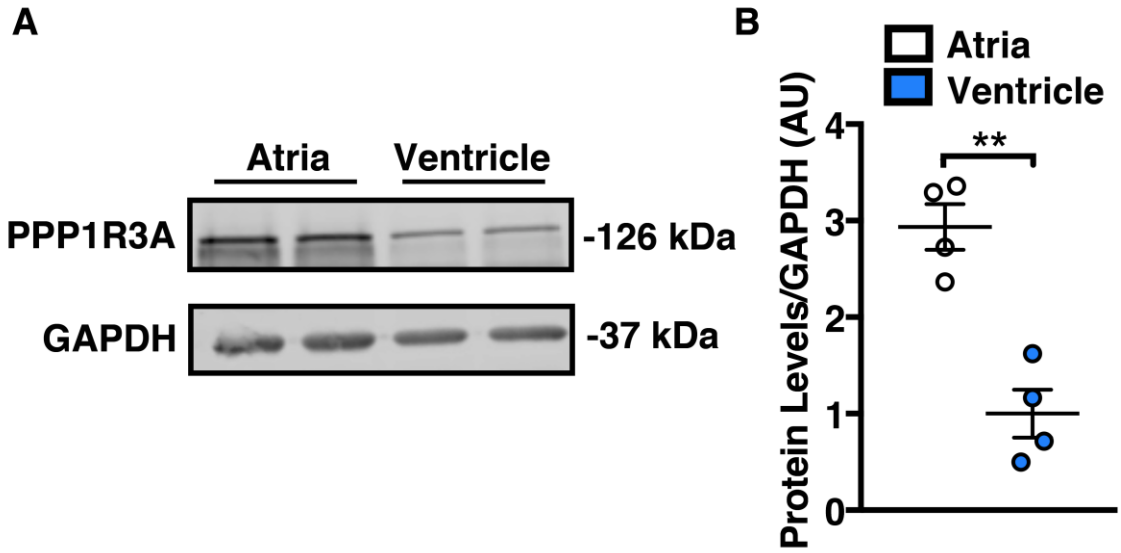

PPP1R3A expression is higher in atria than in ventricle. A and **B,** Representative Western blot images and corresponding dot plot showing that PPP1R3A protein levels are nearly 3-fold higher in atria compared to ventricle of wild-type mouse hearts. Data represent mean±SEM (***P*<0.01 vs. ventricle).

Supplemental Figure 6

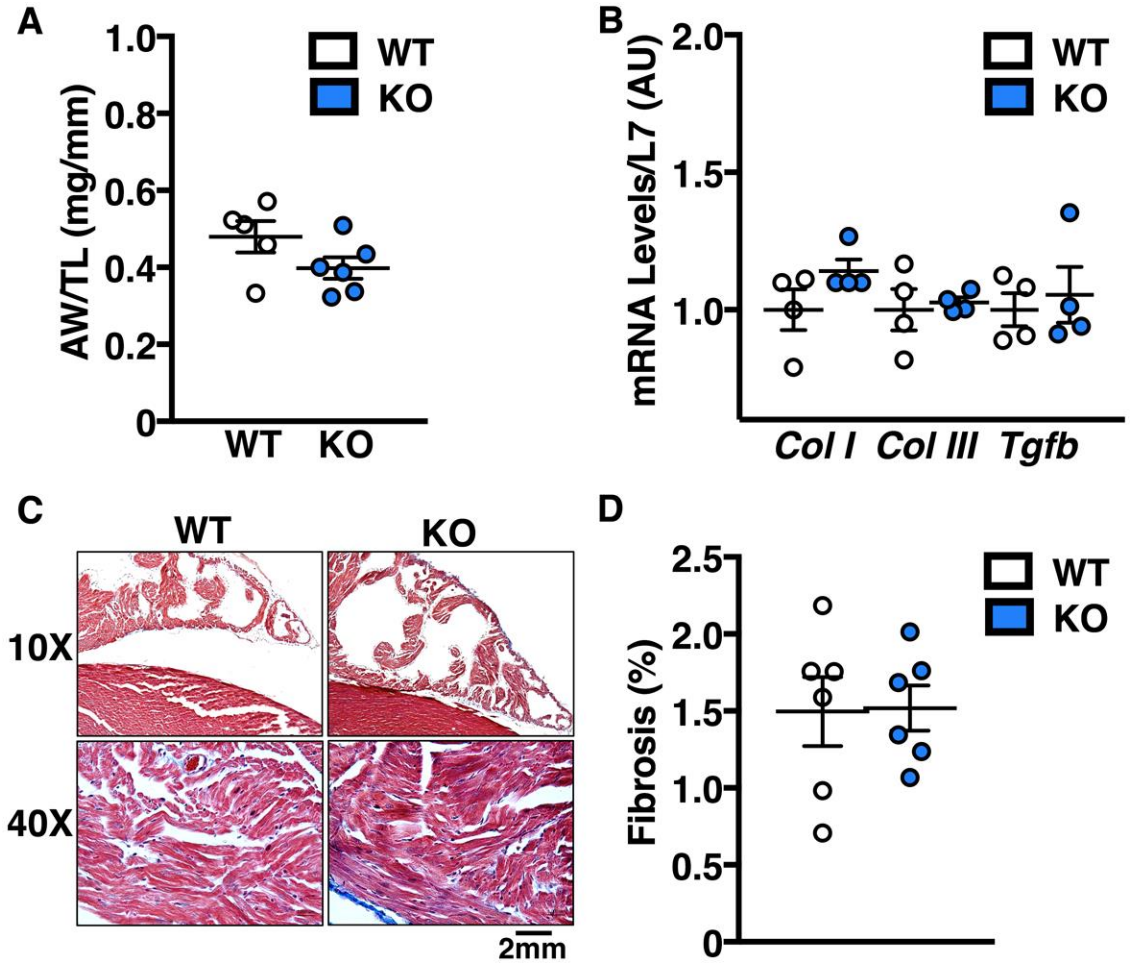

No signs of atrial fibrosis in *Ppp1r3A* KO atria. Summary dot plots depicting (**A**) no change in atrial weight (AW) normalized to tibial length (TL) in *Ppp1r3A* KO mice and (**B**) no change in atrial transcript levels of fibrotic markers collagen-I (*Col I*), collagen-III (*Col III*), or transforming growth factor beta (*Tgfb*) in *Ppp1r3A*-KO hearts. **C** and **D**, Masson trichrome staining confirming no difference in interstitial fibrosis between *Ppp1r3A*-KO and WT atria. Data represent mean±SEM.

Supplemental Figure 7

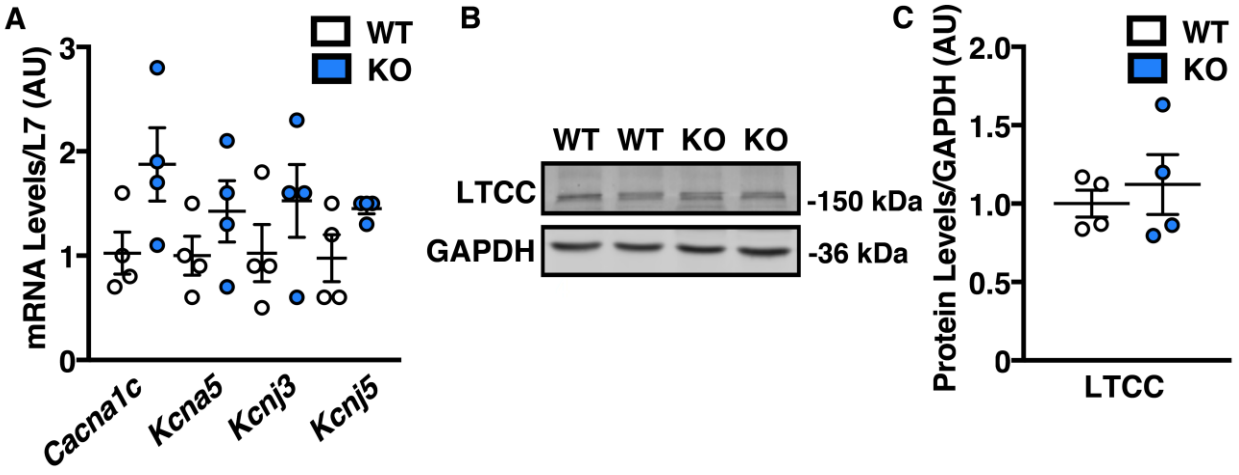

Unaltered ion channel levels in *Ppp1r3a*-KO atria. A, Summary dot plots depicting no significant differences in transcript levels of *Cacna1c*, *Kcna5*, *Kcnj3*, and *Kcnj5* between *Ppp1r3a*-KO and WT atria. **B**, Representative Western blot and (**C**) summary dot plots confirming protein levels of LTCC (encoded by *Cacna1c*) are unaltered in *Ppp1r3a*-KO atria. Data represent mean±SEM.

Supplemental Figure 8

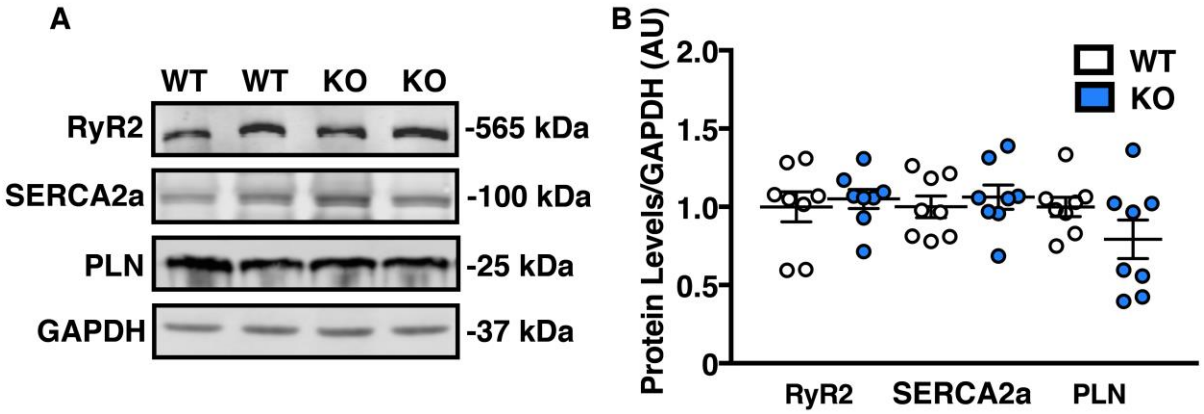

Unchanged protein expression levels of SR Ca^{2+} handling proteins in *Ppp1r3a*-KO atria. A and **B,** Representative Western blot images and corresponding dot plot showing that *Ppp1r3a* ablation has no effect on atrial expression levels of the major SR Ca^{2+} handling proteins RyR2, SERCA2a, and PLN. Data represent mean±SEM.

Supplemental Figure 9

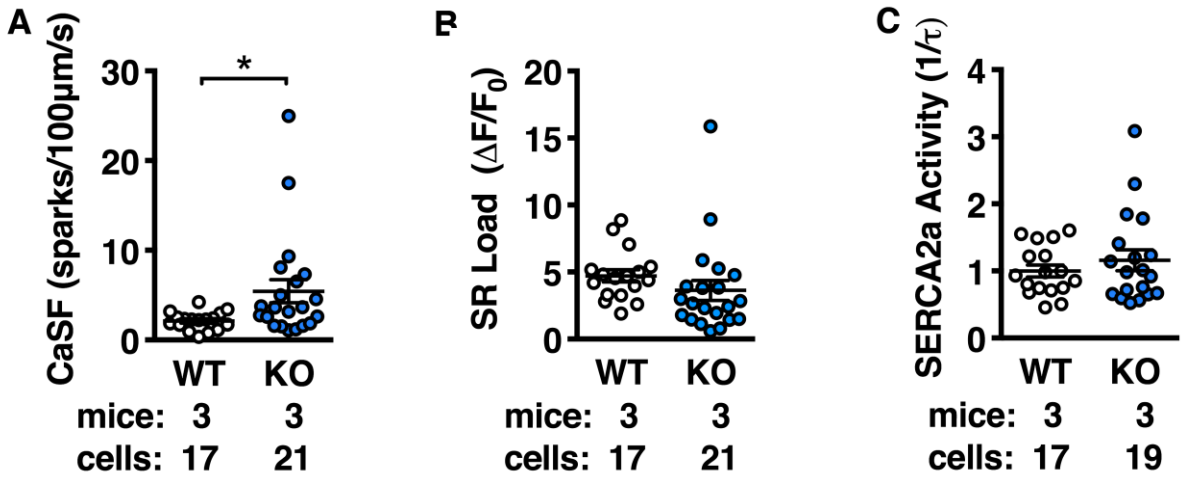

***Ppp1r3a*-KO atrial cardiomyocytes have heightened sensitivity to isoprenaline.** Dot plots summarizing (**A**) spontaneous Ca^{2+} spark frequency (CaSF), (**B**) total caffeine-induced SR Ca^{2+} load, and (**C**), SERCA2a activity following 5-minute incubation in 100nM isoprenaline. Data represent mean±SEM and were analyzed using the Generalized Estimating Equation function in SPSS (*P<0.05 vs. WT).

Supplemental Figure 10

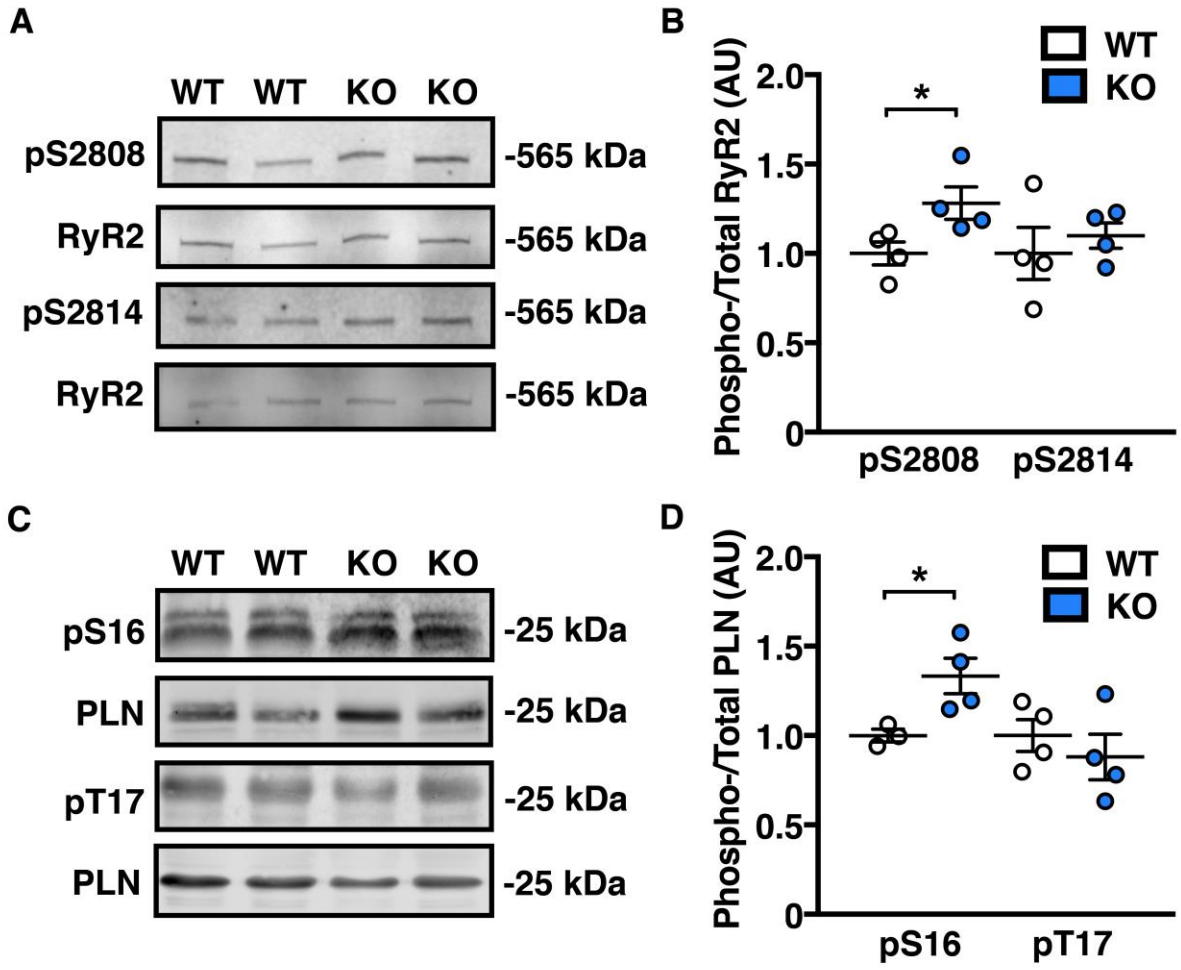

Phosphorylation levels of RyR2 and PLN in *Ppp1r3a*-KO ventricle. Representative Western blot images and corresponding dot plots showing that *Ppp1r3a* ablation leads to (**A** and **B**) increased phosphorylation of ventricular RyR2 at S2808 but not at S2814, and (**C** and **D**) increased phosphorylation of ventricular PLN at S16 but not at T17. Data represent mean±SEM (P<0.05 vs. WT).

Supplemental Figure 11

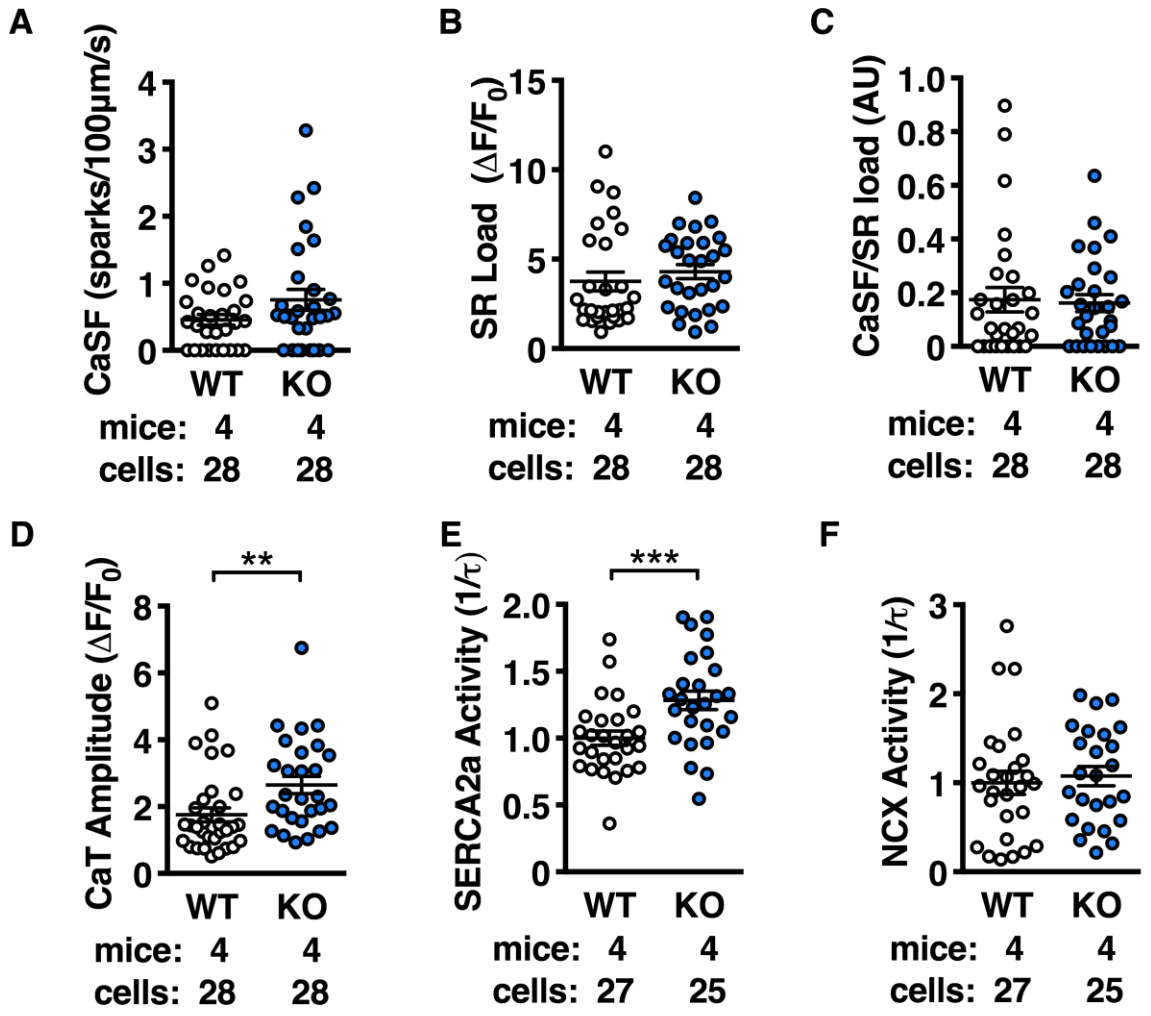

Ca^{2+} handling alterations in ventricular cardiomyocytes from *Ppp1r3a*-KO mice. Upper: Dot plots summarizing (**A**) spontaneous Ca^{2+} spark frequency (CaSF), (**B**) total caffeine-induced SR Ca^{2+} load and (**C**) CaSF normalized to caffeine-induced SR Ca^{2+} load. Lower: Bar graphs summarizing (**D**) Ca^{2+} transient amplitude, (**E**), SERCA2a activity and (**F**) NCX activity. Abbreviations: CaSF, Ca^{2+} spark frequency; CaT, Ca^{2+} transient. Data represent mean±SEM and were analyzed using the Generalized Estimating Equation function in SPSS (***P*<0.01, ****P*<0.001 vs. WT).

Supplemental Figure 12

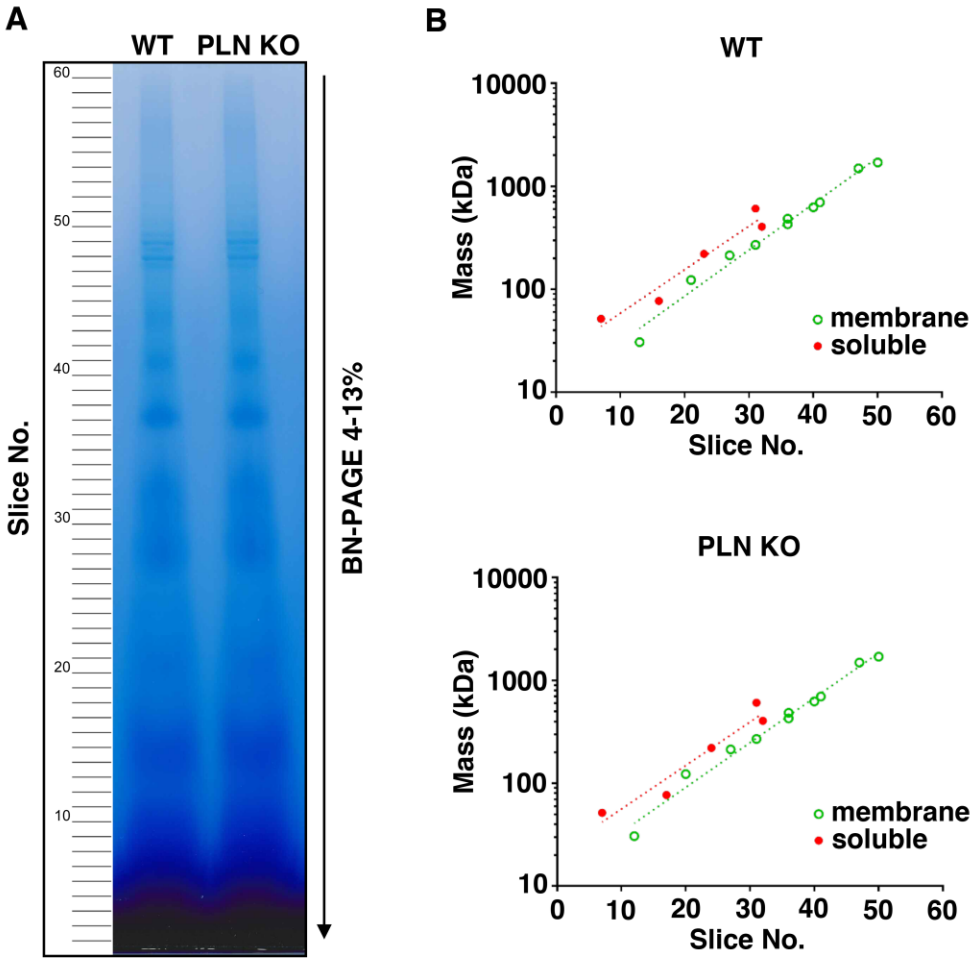

BN-PAGE gel for complexome profiling and mass calibration. A, BN-PAGE gel lanes from WT and PLN KO ventricular cardiomyocytes. The indicated 60 slices were cut and subjected to in-gel tryptic digestion and mass spectrometry. **B**, Mass calibration of soluble and integral membrane proteins and protein complexes in blue native electrophoresis.[15] *Membrane protein standards*: monomeric voltage-dependent anion channel (VDAC) 1 (30.7 kDa), VDAC 1,2,3 heterononameric complex (270 kDa), respiratory complexes II (123 kDa), IV (214 kDa), III2 (485 kDa) and V (626 kDa) and supercomplexes I-III2 (1494 kDa), I-III2-IV (1708 kDa). *Soluble protein standards*: heptameric 60 kDa heat-shock protein (405 kDa), monomeric ATP synthase subunit

beta (51.7 kDa), tetrameric mitochondrial aldehyde dehydrogenase X (221 kDa), isocitrate dehydrogrenase complex (608 kDa), NDUFS1 not bound to other complex I subunits (77kDa).

Supplemental Figure 13

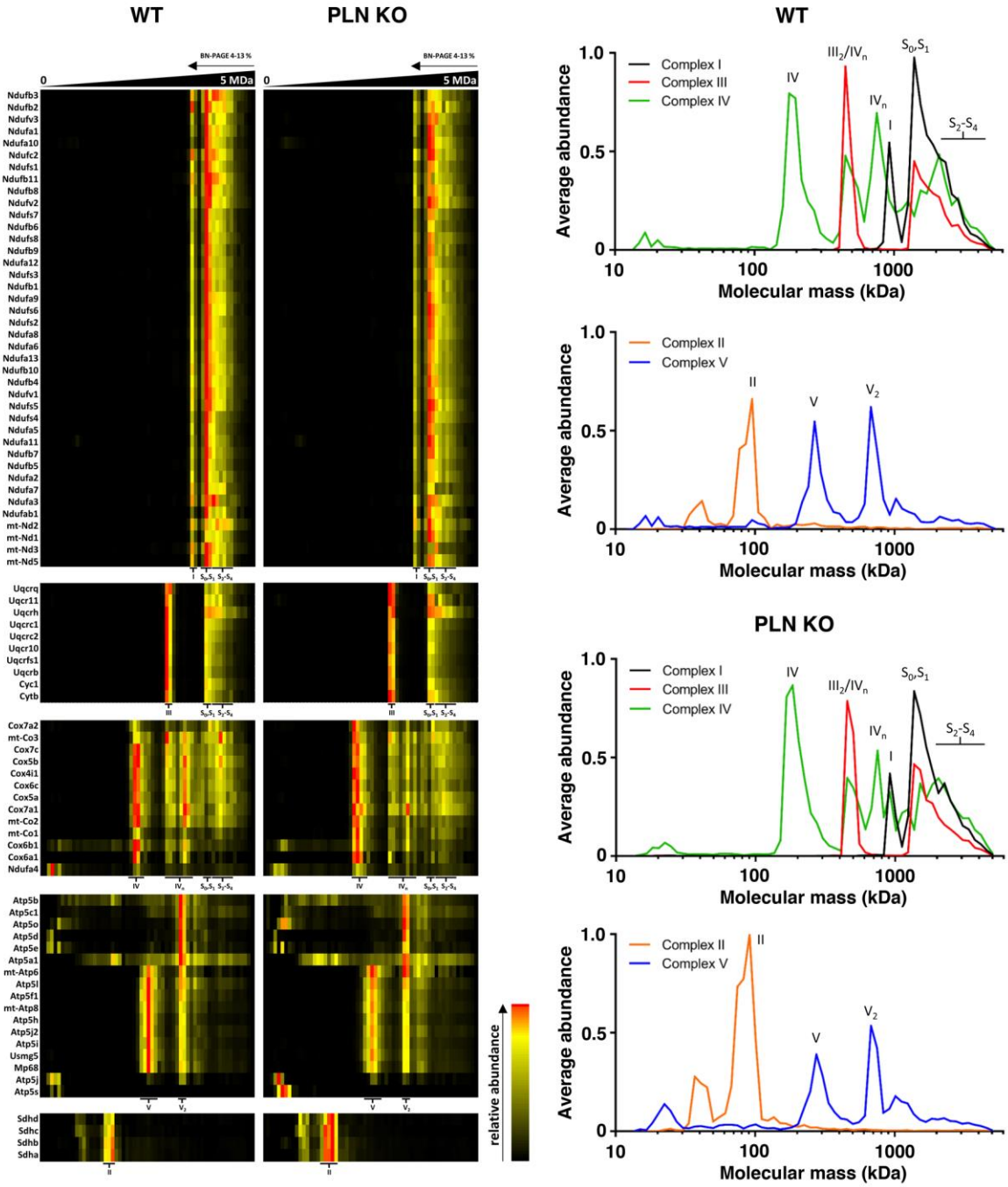

Complexome profiling of OXPHOS complexes. Heat maps (**left**) and migration profiles (**right**) of OXPHOS complexes in PLN WT and KO cardiomyocytes used as methodical quality control and for mass calibration. Respiratory chain complexes are indicated as complex I (I), complex II

(II), complex V (V,V_2, dimer), complex III (III_2, dimer), complex IV (IV, IV_n, multimer) and supercomplexes (S_0-S_4).[16]

Supplemental Figure 14

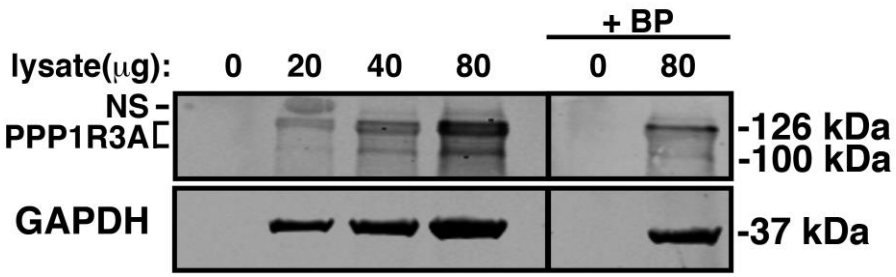

Validation of PPP1R3A antibody in human atrial tissue. Western blot images showing full-length and proteolyzed human PPP1R3A bands running around 126kD and 100kD, respectively, in atrial samples taken from control patients in sinus rhythm. Lysates were either untreated (left) or treated with a PPP1R3A antibody blocking peptide (right). Abbreviations: BP, blocking peptide; NS, nonspecific band.

Supplemental Figure 15

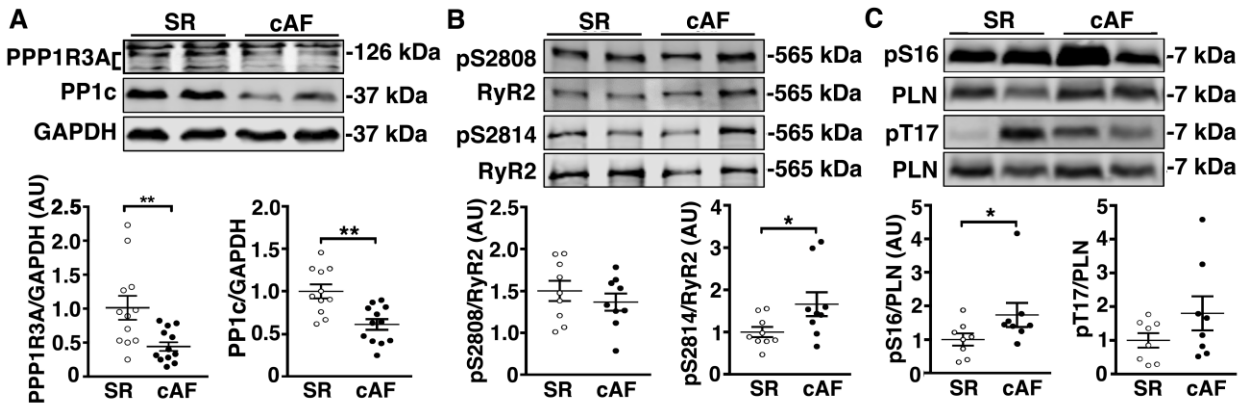

Phosphorylation levels of RyR2 and PLN in cAF patients. Representative Western blots (upper) and corresponding dot plots (lower) showing (**A**), expression levels of PPP1R3A and PP1c, (**B**) phosphorylation levels of RyR2 at S2808 and S2814, and (**C**) phosphorylation levels of PLN at S16 and T17 in atrial tissue from sinus rhythm (SR) vs. cAF patients. Data represent mean±SEM (**P*<0.05; ***P*<0.01 vs. SR).

Supplemental Figure 16

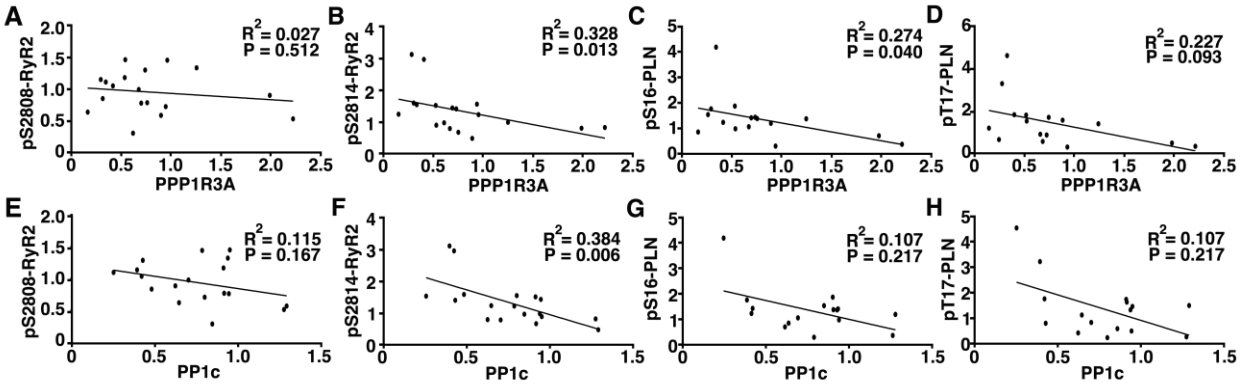

Correlation of PPP1R3A with phosphorylation of RyR2 and PLN in human atria. Scatter plots showing correlation analysis of (**A-D**), PPP1R3A or (**E-H**) PP1c with RyR2-pS2808, RyR2-pS2814, PLN-S16 and PLN-T17 in human atrial tissues. Correlation analysis was performed according to the D'Agostino & Pearson normality test, using Pearson's correlation coefficient or Spearman's rank correlation.

Supplemental Figure 17

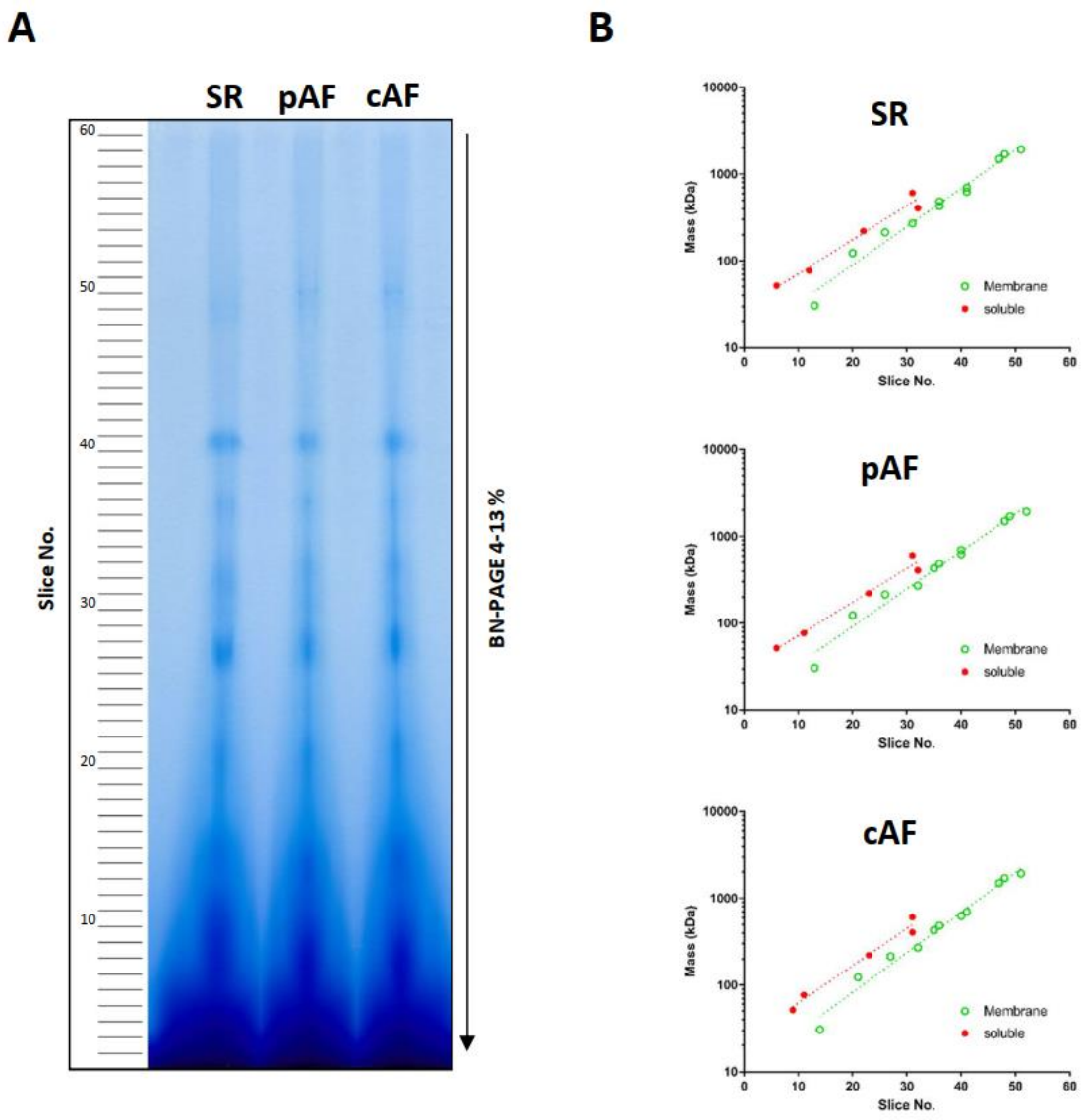

BN-PAGE gel used for complexome profiling and mass calibration of human atrial tissue. **A**, BN-PAGE gradient gel (*right*: 4-13%) showing three lanes of migrating protein complexes isolated from lysed atrial tissue of patients with sinus ryhthm (SR), paroxysmal AF (pAF), or chronic AF (cAF). *Left*: 60 slices of equal size were cut and subjected to in-gel tryptic digestion and mass spectrometry. **B**, Mass calibration for soluble and membrane proteins including protein complexes by blue native electrophoresis[15]. *Membrane protein standards:* monomeric voltage-dependent anion channel (VDAC) 1 (30.7 kDa), VDAC 1,2,3 heterononameric complex (270 kDa),

respiratory complexes II (123 kDa), IV (214 kDa), III2 (485 kDa) and V (626 kDa) and supercomplexes I-III2 (1494 kDa), I-III2-IV (1708 kDa). *Soluble protein standards:* heptameric 60 kDa heat-shock protein (405 kDa), monomeric ATP synthase subunit beta (51.7 kDa), tetrameric mitochondrial aldehyde dehydrogenase X (221 kDa), isocitrate dehydrogenase complex (608 kDa), NDUFS1 not bound to other complex I subunits (77 kDa).

Supplemental Figure 18

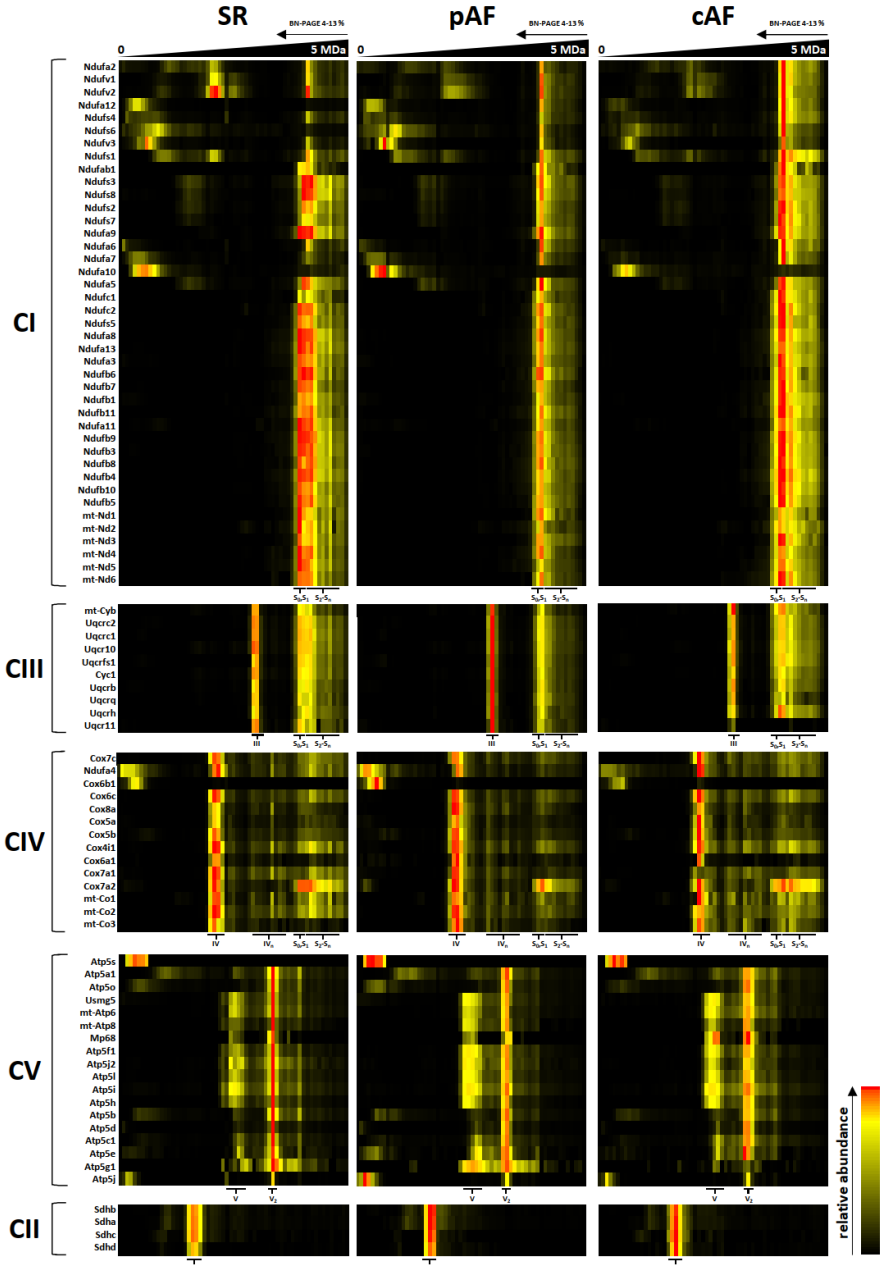

Complexome profiling of human atrial OXPHOS complexes. Heat maps of human OXPHOS complexes from atrial samples of SR, pAF, or cAF patients were used for quality control and calibration purposes. The respiratory chain complexes are indicated as complex I (I), complex II (II), complex V (V,V_2, dimer), complex III (III_2, dimer), complex IV (IV, IV_n, multimer) and supercomplexes (S_0-S_4).[16]

Supplemental Figure 19

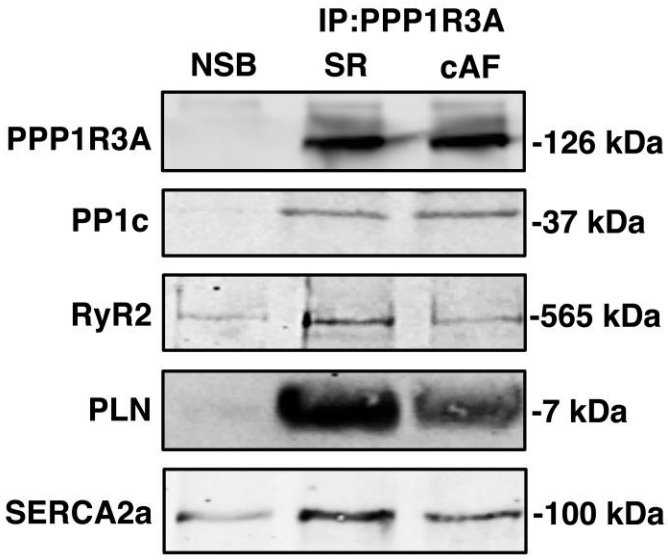

Co-IP of PPP1R3A from human atrial tissues. Representative Western blots showing that PPP1R3A interacts with PP1c as well as with RyR2, PLN and SERCA2a in human atrial tissue from patients in sinus rhythm. Notably, the interaction between PPP1R3A and RyR2, PLN and SERCA2a appears reduced in patients with cAF. Abbreviations: NSB, non-specific binding (to beads).

REFERENCES

1. Hodgkins A, Farne A, Perera S, Grego T, Parry-Smith DJ, Skarnes WC, Iyer V. WGE: a CRISPR database for genome engineering. *Bioinformatics*. 2015;31:3078-3080.
2. Chiang DY, Lebesgue N, Beavers DL, Alsina KM, Damen JM, Voigt N, Dobrev D, Wehrens XH, Scholten A. Alterations in the interactome of serine/threonine protein phosphatase type-1 in atrial fibrillation patients. *J Am Coll Cardiol*. 2015;65:163-173.
3. Cox J, Mann M. MaxQuant enables high peptide identification rates, individualized p.p.b.-range mass accuracies and proteome-wide protein quantification. *Nat Biotechnol*. 2008;26:1367-1372.
4. Li N, Wang T, Wang W, Cutler MJ, Wang Q, Voigt N, Rosenbaum DS, Dobrev D, Wehrens XH. Inhibition of CaMKII phosphorylation of RyR2 prevents induction of atrial fibrillation in FKBP12.6 knockout mice. *Circ Res*. 2012;110:465-470.
5. Chiang DY, Kongchan N, Beavers DL, Alsina KM, Voigt N, Neilson JR, Jakob H, Martin JF, Dobrev D, Wehrens XH, Li N. Loss of microRNA-106b-25 cluster promotes atrial fibrillation by enhancing ryanodine receptor type-2 expression and calcium release. *Circ Arrhythm Electrophysiol*. 2014;7:1214-1222.
6. Chelu MG, Sarma S, Sood S, Wang S, van Oort RJ, Skapura DG, Li N, Santonastasi M, Muller FU, Schmitz W, Schotten U, Anderson ME, Valderrabano M, Dobrev D, Wehrens XH. Calmodulin kinase II-mediated sarcoplasmic reticulum Ca2+ leak promotes atrial fibrillation in mice. *J Clin Invest*. 2009;119:1940-1951.
7. Li N, Wehrens XH. Programmed electrical stimulation in mice. *J Vis Exp*. 2010:1730.
8. Verheule S, Sato T, Everett Tt, Engle SK, Otten D, Rubart-von der Lohe M, Nakajima HO, Nakajima H, Field LJ, Olgin JE. Increased vulnerability to atrial fibrillation in transgenic mice with selective atrial fibrosis caused by overexpression of TGF-beta1. *Circ Res*. 2004;94:1458-1465.

9. Respress JL, Wehrens XH. Transthoracic echocardiography in mice. *J Vis Exp*. 2010;39:1738.

10. Brandenburg S, Kohl T, Williams GS, Gusev K, Wagner E, Rog-Zielinska EA, Hebisch E, Dura M, Didie M, Gotthardt M, Nikolaev VO, Hasenfuss G, Kohl P, Ward CW, Lederer WJ, Lehnart SE. Axial tubule junctions control rapid calcium signaling in atria. *J Clin Invest*. 2016;126:3999-4015.

11. Wagner E, Brandenburg S, Kohl T, Lehnart SE. Analysis of tubular membrane networks in cardiac myocytes from atria and ventricles. *J Vis Exp*. 2014:e51823.

12. Voigt N, Heijman J, Wang Q, Chiang DY, Li N, Karck M, Wehrens XHT, Nattel S, Dobrev D. Cellular and molecular mechanisms of atrial arrhythmogenesis in patients with paroxysmal atrial fibrillation. *Circulation*. 2014;129:145-156.

13. Wittig I, Braun HP, Schagger H. Blue native PAGE. *Nat Protoc*. 2006;1:418-428.

14. Atanassov I, Urlaub H. Increased proteome coverage by combining PAGE and peptide isoelectric focusing: comparative study of gel-based separation approaches. *Proteomics*. 2013;13:2947-2955.

15. Wittig I, Beckhaus T, Wumaier Z, Karas M, Schagger H. Mass estimation of native proteins by blue native electrophoresis: principles and practical hints. *Mol Cell Proteomics*. 2010;9:2149-2161.

16. Heide H, Bleier L, Steger M, Ackermann J, Drose S, Schwamb B, Zornig M, Reichert AS, Koch I, Wittig I, Brandt U. Complexome profiling identifies TMEM126B as a component of the mitochondrial complex I assembly complex. *Cell Metab*. 2012;16:538-549.